

# High Resolution Spectroscopy of the Pulsating White Dwarf G29-38

Susan E. Thompson,<sup>1</sup> J. C. Clemens,<sup>1,2</sup> M. H. van Kerkwijk,<sup>3,4</sup> and D. Koester<sup>5</sup>

sthomp@physics.unc.edu, clemens@physics.unc.edu, mhvk@astro.utoronto.ca,  
koester@astrophysik.uni-kiel.de

## ABSTRACT

We present the analysis of time-resolved, high resolution spectra of the cool white dwarf pulsator, G 29-38. From measuring the Doppler shifts of the H $\alpha$  core, we detect velocity changes as large as 16.5 km/s and conclude that they are due to the horizontal motions associated with the g-mode pulsations on the star. We detect seven pulsation modes from the velocity time-series and identify the same modes in the flux variations. We discuss the properties of these modes and use the advantage of having both velocity and flux measurements of the pulsations to test the convective driving theory proposed for DAV stars. Our data show limited agreement with the expected relationships between the amplitudes and phases of the velocity and flux modes. Unexpectedly, the *velocity* curve shows evidence for harmonic distortion, in the form of a peak in the Fourier transform whose frequency is the exact sum of the two largest frequencies. Combination frequencies are a characteristic feature of the Fourier transforms of light curves of G 29-38, but before now have not been detected in the velocities, nor does published theory predict that they should exist. We compare our velocity combination frequency to combination frequencies found in the analysis of light curves of G 29-38, and discuss what might account for the existence of velocity combinations with the properties we observe.

We also use our high-resolution spectra to determine if either rotation or pulsation can explain the truncated shape observed for the DAV star's line core. We are able to eliminate both mechanisms: the average spectrum does not fit the rotationally broadened model and the time-series of spectra provides proof that the pulsations do not significantly truncate the line.

*Subject headings:* white dwarf, stars:variables:other, stars:individual (G 29-38), stars:scillations, stars:rotation

## 1. Introduction

G 29-38 (ZZ Psc) is an extensively observed V=13.05 magnitude pulsating white dwarf that lies at the cool end of the DA instability strip. Like many cool DAV stars, its oscillation properties are highly variable. In one month it may exhibit a dominant period of 615 s and amplitudes of 6% (Winget et al. 1990).

---

<sup>1</sup>Department of Physics and Astronomy, University of North Carolina, Chapel Hill, NC 27599-3255, USA

<sup>2</sup>Alfred P. Sloan Research Fellow

<sup>3</sup>Astronomical Institute, Utrecht University, PO Box 8000, 3508 TA Utrecht, Netherlands

<sup>4</sup>Present address: Department of Astronomy and Astrophysics, University of Toronto, 60 St. George Street, Toronto, ON, M5S 3H8, Canada

<sup>5</sup>Institut für Theoretische Physik und Astrophysik, Universität Kiel, 24098 Kiel, Germany

In another month it may have a dominant period of 809 s and amplitudes of 4% (Kleinman et al. 1998). Occasionally it shows no measurable pulsations at all. In addition to being confusing in themselves, these amplitude changes frustrate attempts to identify eigenfrequencies that might allow seismological analysis of the internal structure of G 29-38.

Kleinman et al. (1998) accomplished a breakthrough in seismology of G 29-38 by compiling and analyzing many months of time-series photometric observations. They found a consistent pattern of recurring frequencies in the data. This result is reassuring to seismologists because it suggests that the observed frequencies represent eigenfrequencies that carry information about internal structure. Kleinman et al. (1998) and Bradley & Kleinman (1997) presented an analysis of the pattern of modes, concluding they are most likely modes of the first spherical harmonic degree ( $\ell = 1$ ). The conclusion was based on the match of the spacing between modes to theoretical expectations for  $\ell = 1$  modes of consecutive radial eigennumber, and upon the observation of triplet structure in some of the modes. Rotation should split  $\ell = 1$  modes into three components of different azimuthal quantum number ( $m$ ). Seismological analysis of the mode pattern yielded a mass estimate of  $0.6M_{\odot}$  for an assumed Hydrogen layer mass of  $10^{-4}M_{\star}$ .

Kleinman et al. (1998) had no way to verify their mode identification by direct observation, but subsequent time-series spectroscopy at high signal-to-noise by Clemens, van Kerkwijk, & Wu (2000) provided verification for some modes. Because of the wavelength dependence of limb darkening, pulsation amplitudes at each color are sensitive to the degree ( $\ell$ ) of pulsation modes. Using time-resolved spectroscopy from Keck II LRIS (Oke et al. 1995), Clemens et al. (2000) confirmed that most of the modes are  $\ell = 1$ . The only exception is a mode at 777 s that Clemens et al. (2000) identify as  $\ell = 2$ .

In addition to mode identification, van Kerkwijk, Clemens, & Wu (2000) detected velocity shifts associated with pulsations of G 29-38, and thereby obtained the first direct measurements of the size of the surface motions in a pulsating white dwarf. Because surface velocities are distributed as the derivative of a spherical harmonic, their integrated contribution does not cancel in the same way as the spherically distributed flux variations. As a result, the ratio of velocity to flux amplitudes is sensitive to  $\ell$ , and measurements of these ratios also support the conclusion that the 777 s mode is  $\ell = 2$  and the remainder  $\ell = 1$ . Later, Kotak, van Kerkwijk, & Clemens (2002) showed that the 918 s mode observed by van Kerkwijk et al. (2000) also has  $\ell = 2$ .

Encouraged by the success of the LRIS observations (van Kerkwijk et al. 2000), we aspired to improve the velocity measurements by observing at higher resolution. Accordingly, we obtained a 5 hour time-series of the  $H\alpha$  core of G 29-38 with the Keck I High Resolution Echelle Spectrograph (Vogt et al. 1994, HIRES). We used a narrow slit to improve the velocity measurements of G 29-38 at the expense of some quality in the flux measurements. Using this technique, we have successfully detected the pulsation velocities, confirming the LRIS observations of van Kerkwijk et al. (2000), and we have achieved a signal-to-noise in the velocity curve better than any previous measurements. In this paper we use our higher precision measurements to examine questions concerning the ZZ Ceti driving mechanisms, combination modes, and the shape of the ZZ Ceti  $H\alpha$  line.

Recent theories of ZZ Ceti mode excitation make specific predictions about the relative sizes of velocity and flux variations. Our simultaneous measurements of each allow us to test the predictions. Originally, the classical  $\kappa - \gamma$  mechanism was proposed as a plausible driving mechanism for the pulsations (Winget et al. 1982; Dziembowski & Koester 1981; Dolez & Vauclair 1981). Later, Brickhill (1983, 1991) recognized that the convection zone responds immediately to the flux perturbations from the radiative interior and demonstrated that the convection zone could be the center of mode driving. His convective driving mechanism, as further

developed by Goldreich & Wu (1999), makes explicit, testable predictions concerning the relationship between the phases and amplitudes of the observed modes. Our measurements agree with the basic predictions of this model, but are not sufficient to provide rigorous tests of how mode qualities change with frequency.

Our observations also enable us to explore the harmonic distortions frequently observed in G 29-38. The distinct shape of ZZ Ceti light curves have been a puzzle since Warner & Nather (1970) published the first time-series photometry of HL Tau 76. Small-amplitude ZZ Ceti pulsators, now identified as the hotter members of the class, have nearly sine-like photometric variations, but the cooler, large-amplitude pulsators show distinctive non-sinusoidal shapes, with broad, flat minima and sharp maxima (see Figure 1). Corresponding to these shapes are the appearance of sum and difference frequencies in the Fourier spectrum.

Theoretical calculations, first by Brickhill (1983, 1992), and later by Wu (2001) and Ising & Koester (2001), explain this phenomenon within the context of the convective driving theory. Brickhill built a numerical model of a ZZ Ceti surface convection zone and showed that sinusoidal flux variations at its base are attenuated and delayed in phase before reaching the surface. Moreover, because the thickness of the model convection zone decreases between flux minimum and flux maximum, the amount of attenuation and delay changes within a cycle. This non-linearity distorts the sinusoidal input variation into a surface flux variation whose shape in the model is similar to that we observe. Wu (2001) has found the same result analytically, while Ising & Koester (2001) have confirmed and extended the numerical results of Brickhill (1983).

Other theories for the origin of the pulse shapes invoke the non-linear relationship between flux and surface temperature ( $F \propto T^4$ ; see Brassard, Fontaine, & Wesemael 1995), or the excitation of independent pulsation modes by resonant mode coupling. In a recent series of papers, Vuille and collaborators show that the former theory cannot account for the large sizes of the combination frequencies in the large amplitude pulsator G 29-38 (Vuille & Brassard 2000) and the latter cannot naturally explain the phasing of modes with their combinations (Vuille 2000b). They conclude that the majority of combination frequencies in G 29-38 and, by inference, the other large amplitude pulsators arise from harmonic distortion like that described in the models of Brickhill (1983, 1992), Wu (2001), and Ising & Koester (2001).

Our measurements complicate matters further by revealing the first combination frequency in the Fourier transform of the *velocity* curve of a ZZ Ceti star. This detection is a surprise, because Brickhill (1983) and Wu (2001) both maintain that surface velocities should not be distorted by the convection zone in their models. We will speculate about what might account for our observations, using the relative phase of the velocity combination we have measured as our only clue. Because we have detected only a single combination peak, we will require more observations to establish whether or not its properties are typical of large amplitude ZZ Ceti pulsations.

Finally, our spectra of G 29-38 help us explore another mystery, associated with the shape of the H $\alpha$  core in the mean spectrum of DAV stars. Koester et al. (1998) observed the NLTE H $\alpha$  core profiles for 28 DA white dwarfs in order to measure their rotation rates. For the majority of DA stars, they measured line cores consistent with  $v \sin i$  of 15 km/s or less, but for all 3 ZZ Ceti stars in their sample (including G 29-38) and one star just below the instability strip, they found shallow line cores requiring velocities of 29-45 km/s. Not only are rotation speeds of this size too high for the rotation period suggested by triplet splitting in the Kleinman et al. (1998) study, but they require that the ZZ Ceti stars as a group rotate much faster than other DA stars. This would indicate that ZZ Ceti stars are either not ordinary DAs or their rotation rate increases when they cool into the instability strip. Our mean spectrum confirms the measurements of Koester et al. (1998), and we explore whether the Doppler shifts associated with the pulsations could cause the unusual

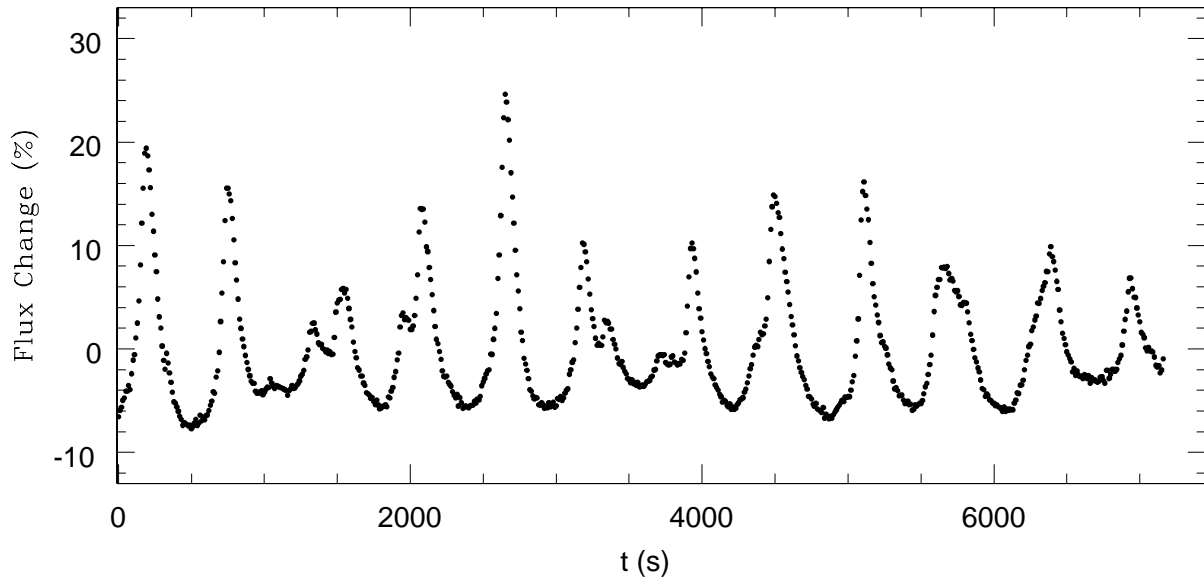


Fig. 1.— A typical light curve of G 29-38 showing the non-sinusoidal character of the pulsations, courtesy of the Whole Earth Telescope data archives. These data were obtained by M. Wood using the 82" Struve telescope at McDonald Observatory and a Nather two-star photometer with 10 s sampling times.

line shape for G 29-38.

The paper is organized in seven sections. In the next section (§2) we describe the observations and the method used to reduce the spectral images into velocity and flux curves. In §3 and §4 we examine the modes revealed via Fourier analysis and discuss the results in the context of the convective driving model. In §5 we discuss the combination frequency discovered in the velocity curve. In §6 we compare our average spectrum to that of Koester et al. (1998) and discuss the cause of the anomalous line core. Finally, we present our conclusions in §7.

## 2. Observations and Reduction

On September 16, 1997, we acquired a series of 236 spectra of G 29-38 using HIRES (Vogt et al. 1994) on the Keck I telescope. We used the red collimator, the KV408 order blocking filter, and the C2 decker, which yielded a slit width of  $0.861''$ . In this configuration, the 24-micron pixel Tektronix 2048EB2 CCD with  $2 \times 2$  binning gave a dispersion of  $0.095 \text{ \AA}$  per binned pixel, and a scale of  $0.38''$  per binned pixel in the spatial direction. The effective spectral resolution, defined by the slit width, was  $0.215 \text{ \AA}$ .

We began our 5 hour sequence of exposures at 08:28:02 UT (measured by the observatory clock and recorded in the image headers). The exposure time for each spectrum was 50 seconds with an additional 28 seconds required to read and wipe the CCD, yielding a duty cycle of 64%. Since reading the entire CCD would have taken much longer and thus unacceptably reduced the duty cycle, we only read a region containing three orders (53, 54, and 55) with the middle order centered on  $H\alpha$ . For this small region, the readout time with two amplifiers was not significantly better than with one, so we used one amplifier to eliminate complications arising from differences in gain and linearity. The exposure levels in our 50 second integrations ranged from 35 electrons in the core of  $H\alpha$  to 70 in the wings. The moon was full, so the background sky was relatively high, ranging from 16 to 40 electrons with clearly visible features of the solar spectrum, and the shot noise from the sky is comparable to the read noise of 4.5 electrons. In Figure 2 we show a raw spectral image for the average of all 236 images. We reduced only the central order since we were interested in the  $H\alpha$  line and did not need the extended continuum in the other orders.

We acquired well-exposed spectra of a halogen lamp to use for spectral flats and of a Thorium-Argon lamp to use for wavelength calibration. We also acquired spectra of the flux standard G 126-18, but in this paper we present only relative photometry, and have made no attempt at absolute flux calibration.

The seeing during our run, as measured from spatial profiles, averaged about  $1.2''$  fwhm, so the relatively narrow slit makes photometry problematic. Moreover, to avoid introducing potential periodic variations, we

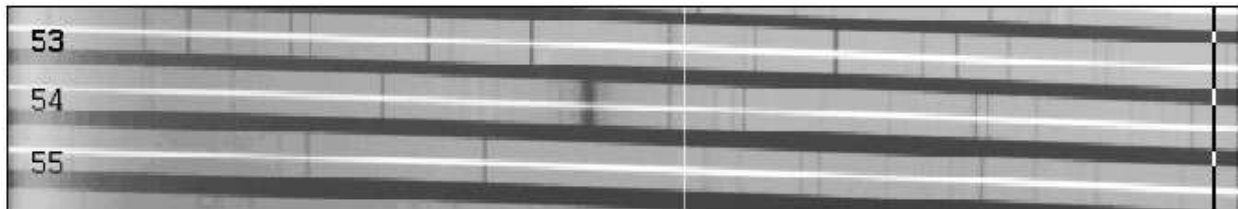


Fig. 2.— The average of the spectral images prior to reduction. The echelle orders are labeled on the left.  $H\alpha$  is located at the center of the 54th order.

did not use the image rotator; so differential refraction slowly changed the amount of light passing through the slit. As we shall see, these losses did not prevent us from measuring periodic variations in the brightness of G 29-38.

We reduced our 236 spectral images using standard Image Reduction and Analysis Facility (IRAF) routines (Tody 1986). We removed the bias level by fitting and subtracting a plane to the prescan region of each image. We removed the blaze function and the flat field variations in one step by dividing the data by the normalized average of the halogen lamp exposures. Normalization was accomplished by dividing the average image by the mean pixel value of the image. To extract individual spectra, we first calibrated our extraction parameters using the average spectrum (see Figure 3) and the IRAF `apall` routine. This gave values for the slope, curvature, and spatial profile of the average spectrum. We assumed individual spectra would have similar values, but might be shifted along the slit, and conducted optimal extraction (Horne 1986) of the lower signal-to-noise, individual spectra with spatial position as the only free parameter. The measured motion of G 29-38 along the slit provides an estimate of the motion across the slit; we used these to assess the slit losses and wavelength stability.

Figure 3 shows a typical individual spectrum after reduction and wavelength calibration. The signal-to-noise is about 8 in the wings of the line and 5 in the line core. The lower panel shows an average of all 236 spectra and was constructed by averaging the reduced spectral images and performing a single extraction. We extracted two time-series from the individual spectra, one representing the changes in velocity and the other representing changes in flux.

To examine the line-of-sight velocity modes on the star, we measured the Doppler shift of the  $H\alpha$  line in each spectrum. Attempts at using cross-correlation against a smoothed average spectrum yielded inconsistent results; the amplitude of the shift was skewed by the amount of the spectrum included in the correlation. As an alternative, we fitted each spectral line to obtain the location of the central wavelength. A Gaussian and Lorentzian, forced to have the same central wavelength, super-imposed on a linear continuum, were fit to the average spectrum over the range 6557.5-6570.0Å. Using this description of the line, we fit the average spectrum until no significant improvement in chi-square was achieved. We obtained a reduced chi-square of about 0.5, indicating a good fit. We then fit each individual spectrum using the average spectrum’s fit as the initial conditions; allowing only the central wavelength, the height of the continuum, the slope of the continuum, and the flux contained in both the Gaussian and Lorentzian to vary for each fit. The width of the Gaussian and the Lorentzian were fixed to the average spectrum’s fitted values. A subtraction of the central wavelength, established with the average spectrum, yielded the spectral shift for each spectrum, and thus line-of-sight velocities. We observe Doppler shifts as large as 0.36Å (3.8 binned pixels), corresponding to a velocity of 16.5 km/s. Figure 4a shows the velocity curve resulting from this reduction.

To obtain the relative changes in the flux of the star, we summed each spectrum from 6553 to 6573 Å and divided the resulting light curve by the mean of these values. The light curve, presented in the lower panel of Figure 4, is normalized by a second order polynomial fit in order to remove long period variations introduced by extinction and differential refraction and yield fractional changes in flux. We observe flux variations as large as 20% from the mean flux. Two sections of the light curve, as indicated in Figure 4, appear to be obstructed by clouds and thus not included in the analysis of the light curve. Increased sky levels concurrent with the decrease in star light confirms this conclusion for the latter region. The Fourier transform and least squares fits of the light curve in §3 do not include these regions.

We measured the effect of flexure on our data by performing this same fitting technique on the spectrum of the sky background in each spectrum. The central wavelength of the sky showed little trend and only

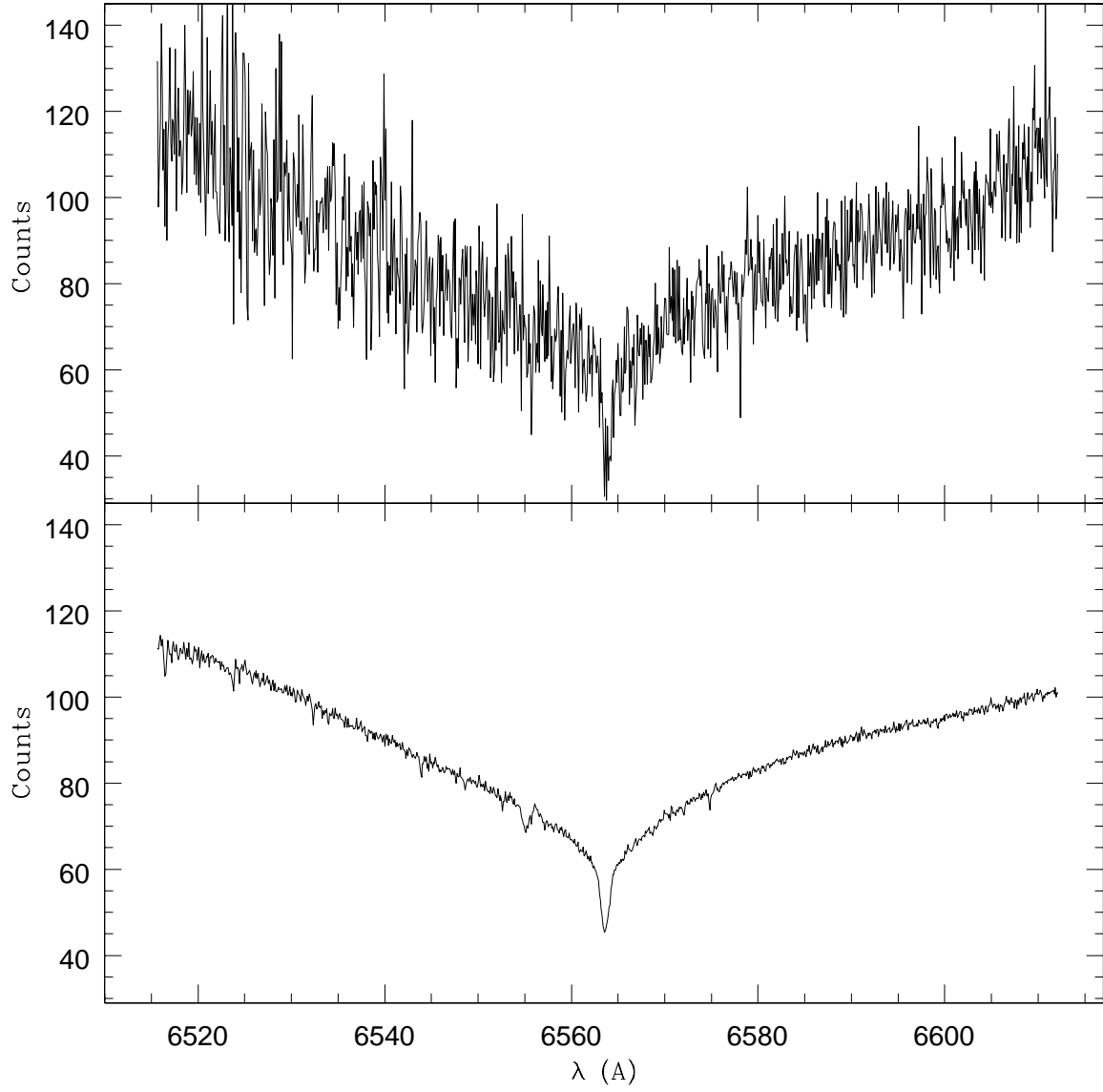


Fig. 3.— An example of an individual spectrum (top panel) and the spectrum extracted from the average of all 236 spectral images (bottom panel). The dominant feature at 6555 Å is due to scattered light. Other features are telluric water lines.

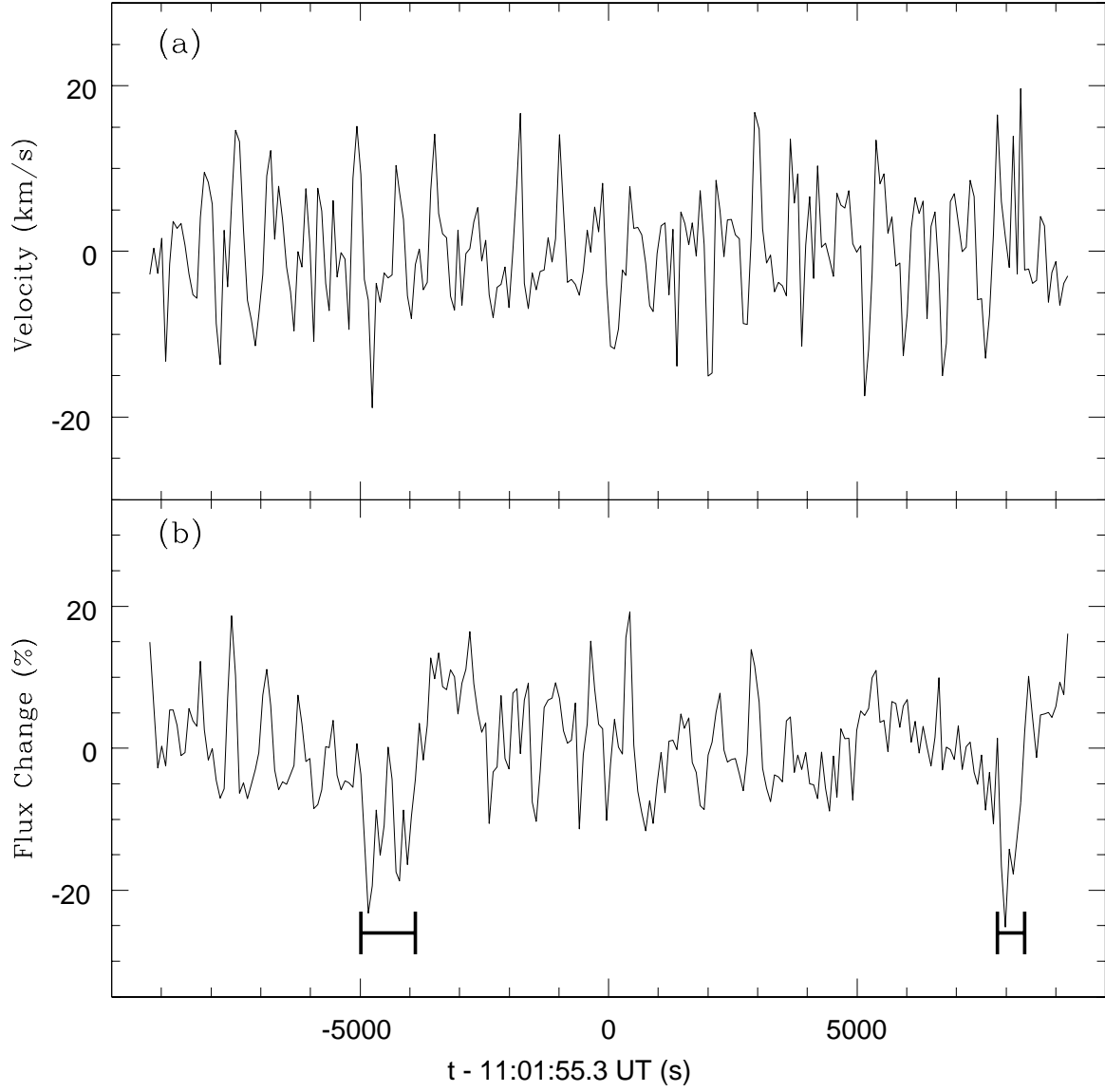


Fig. 4.— (a) The line-of-sight velocity curve, where a positive velocity indicates a red shift. A typical error on a velocity measurement is 3 km/s. (b) The change in flux normalized by a fitted parabola. The marked regions are not used in the Fourier transform or the least-squares fits of the flux curve.



varied by at most 0.2 pixels ( $\sim 1$  km/s).

To be certain the velocities detected are not due to the star moving perpendicular to the slit, we estimated the loss of light that would also result from this motion. We fitted a Gaussian distribution to the spatial profile and assumed the same profile in the dispersion direction (correcting for the different spatial scales). For a  $0.36 \text{ \AA}$  shift (16.5 km/s), the largest detected spectral shifts, we would expect to see flux variations as large as 30% correlated with the shifts. The largest measured flux variations are less than 20% and are not concurrent with the largest spectral shifts. Furthermore, if stellar wander caused the observed spectral shifts, we would expect to see peaks at half the period of the velocity modes. Looking ahead to the Fourier transforms of the velocity and flux variations (Figure 5), we do not see peaks of this sort. Thus, we conclude that stellar motion in the slit is not the primary source of the detected wavelength shifts.

### 3. Flux and Velocity Periodicities

We began analysis of the velocity and flux time-series by investigating the periodicities present in both. Figure 5 shows the Fourier transforms (FTs) of the velocity and flux curves introduced in §2. The three dominant modes in both curves appear at approximately the same frequencies, indicating that the velocity and flux modes are correlated. As such, our data confirm the results of van Kerkwijk et al. (2000), showing significant line-of-sight velocity variations due to the g-mode pulsations on the star.

To further convince ourselves that these Doppler shifts exist in the spectra, we averaged together individual spectra with similar velocities. Figure 6 shows two spectra created by averaging together 30 spectra fit with large positive velocities (red-shifts greater than 6.9 km/s) and 30 spectra with large negative velocities (blue-shifts greater than 6.9 km/s). A noticeable wavelength shift in the center of the line can be seen between these two averages. Hence, we conclude that these Doppler shifts are indeed apparent in the data and not just artifacts of the fits.

The noise level in our velocity curve is significantly better than that measured by van Kerkwijk et al. (2000) while the noise in the flux is worse. This is expected since our technique used a narrow slit to improve velocity measurements at the expense of flux. Our lower noise velocity curve makes the detection and identification of frequencies more reliable relative to our flux measurements. Moreover, there are significant peaks in the velocity transform with no apparent counterparts in the flux transform. Consequently, we analyzed the velocities first and then fitted the flux amplitudes under the assumption that the modes identified have the frequencies measured in the velocity transform.

We began by identifying the periodicities in the velocity curve and removing them consecutively in order of decreasing amplitude. Using the FT’s value for the frequencies and phases as the initial conditions, the velocity curve was fit to a function of the form  $A_v \cos(2\pi ft - \Phi_v) + C$  where  $A_v$  is the amplitude,  $f$  is the frequency,  $\Phi_v$  is the phase and  $C$  is a constant offset. We removed this fitted cosine wave from the data and then repeated the process by identifying the next frequency until no significant peaks could be determined from the Fourier spectrum. A final simultaneous fit of the data to a linear combination of the cosine waves for all identified frequencies yielded the values for  $A_v$ ,  $f$  and  $\Phi_v$  (Table 1). We used the average of the time stamps on the 236 spectra (11:01:55.3 UT) as the zero point for determining the phase.

We estimated the expected noise in the velocity time-series by considering two components: one from the wandering of the star’s position within the slit and the other from our ability to fit the line center in the relatively noisy individual spectra. By measuring the motions of the star along the slit, and removing

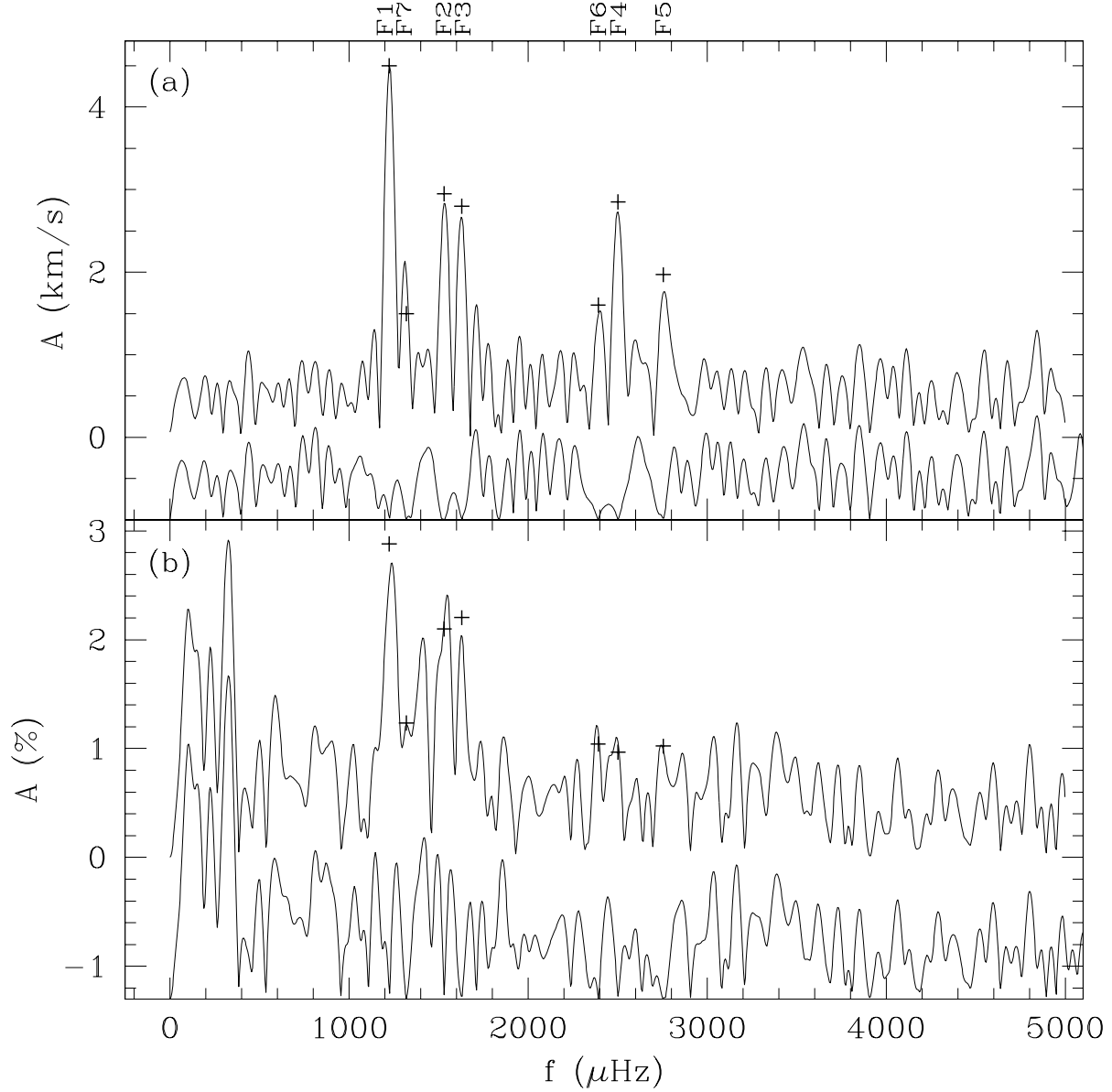


Fig. 5.— The amplitude Fourier transforms of the line-of sight velocity curve **(a)** and relative flux curve **(b)**. The seven modes are marked at the extracted values in both FTs. The amplitude FTs of the residuals are plotted below each FT. The flux residual is off-set by 1.3% while the velocity residual is off-set by 1.0 km/s. The low frequency peaks not extracted from the flux transform are probably atmospheric effects and not inherent to the star.

a parabola to account for slow changes in position with airmass, we constructed an estimate of the rms amplitude of the motions. If we assume that motions across the slit have the same amplitude, this translates into an rms velocity error of 0.4 km/s with the largest extent being 1 km/s (0.36 pixels spatially). To assess the possible impact of periodic wandering, we calculated a Fourier transform of the motions. It shows significant peaks at various guiding frequencies, but they are all far smaller (a factor of 10 to 20 times) than the velocity amplitudes detected in G 29-38 and do not have the same frequencies. The formal error of our velocity fits to individual spectra is  $\sim 3.8$  km/s, much larger than the errors from slit motions. If we assume these are Gaussian, then they should translate into an average noise in the fourier transform of 0.5 km/s. Using this noise level, our fits to the velocity curve yield a reduced chi-square of about 1.4, confirming that 0.5 km/s is a slight underestimate of the noise. We can get a separate estimate of the noise by averaging the power in the 3.5-5.0 mHz region of the velocity FT. This yields an error of  $\sim 0.6$  km/s. We believe that the slight excess may be intrinsic variations due to the low-amplitude pulsations, which are known to exist in this frequency range. The noise level of 0.6 km/s gives a reduced chi-square of about 1.0; we use this noise level to determine the errors reported in Table 1.

To determine the significance of the identified velocity peaks, we conservatively used the noise level determined from the background average power of the FT (0.6 km/s). As such, all 7 modes lie at or above  $3\sigma$ . However, to be certain that these amplitudes could not occur by chance, we calculated the false alarm probability (Horne & Baliunas 1986; Kepler 1993). The five largest velocity modes have less than 1% chance of only being due to noise. The significance of F6 and F7 are questionable since they have a false alarm probability of  $\sim \frac{1}{2}$ . They appear more significant in the FT because the side lobes of the F1 and F4 modes respectively increase their apparent size.

After completing our fits to the velocity curve, we extracted the periodicities in the flux curve by fitting it with a combination of cosine waves, fixing the frequencies to the fitted velocity frequencies. Table 1 contains the amplitudes and phases for the seven modes extracted using this technique. The low frequency peaks in the flux FT are not included since they are not present in the velocity curves and likely result from atmospheric effects, and from an observational technique not optimized for flux measurements. Consequently, the flux curve is not well accounted for by the linear combination of the seven cosine waves. To obtain the errors from the fit we scaled up the error on each measurement to obtain a reduced chi-square of 1. This is reflected in the errors presented in Table 1.

Since we measured the flux modes by fixing the frequencies to the velocity mode frequencies, we determined their significance by calculating the odds that noise would create a peak of that amplitude at the exact frequency we expected to see one. We estimated the noise level from the average of the flux power FT in the region from 3.5-5.0 mHz to be 0.5%. The smallest flux peaks (F4, F5, and F6) lie around  $2.3\sigma$  and have a 2% probability that Gaussian distributed noise would show a peak of that power at the expected frequency.

The frequencies we have measured are all similar or identical to g-mode frequencies previously measured in flux variations of this star. The mode F4 is almost, but not exactly, two times the largest mode F1. Both of these modes are listed in the tabulated photometric modes for G 29-38 (see Kleinman et al. 1998; Vuille 2000a) Near-resonances of this sort are common in the large amplitude ZZ Ceti stars (e.g. BPM 31595; O’Donoghue, Warner & Cropper 1992) but not understood. They do not originate from harmonic distortion of pulse shapes, because that mechanism generates exact frequency combinations.

However, the velocity signal at F5 is the exact sum of the two largest frequency modes (F1+F2) to within the measurement error, as we might expect from pulse shape distortion. We do not see any other

combinations or harmonics in the spectrum. It is quite common in flux measurements to see a signal at the sum of two large modes, but not be able to detect their individual harmonics. In this respect, the velocity transform of Figure 5 resembles a typical flux transform for G 29-38. However, the existence of a velocity combination peak presents a challenge for the convective driving theory, which does not predict distortion in velocity variations. We discuss a possibility for answering this challenge in §5 below.

Because F5 is unexpected, we have worried about possible non-linearities in our fitting procedure that might generate a false combination signal. If the spectral fitting process is non-linear in some way, or if it is biased by the flux, which is varying at the same frequencies but different phase, then harmonics or combination frequencies might be generated as artifacts during the analysis. We have experimented with different fitting routines and also applied cross correlation between the average spectrum and each individual spectrum. In every case, the time series shows a signal at F5, although its significance is sometimes lower. Furthermore, none of the techniques generates combinations or harmonics of other modes in the Fourier transform. We conclude that F5 is a combination frequency present in the star, but emphasize the need for further observations to establish whether velocity combinations are a persistent feature of large amplitude ZZ Ceti pulsators. The first measurement of pulsational velocities by van Kerkwijk et al. (2000) did not show velocity combinations, but the signal-to-noise in their velocity curve was less than one-half of ours, and they would not have been able to detect a signal the size of our F5.

#### 4. Testing the Convective Driving Theory

With the amplitudes and phases of the seven detected pulsation modes, we have knowledge of the motions and the temperature changes at the surface of this ZZ Ceti. The usefulness of these measurements goes beyond calibrating the size of the velocity variations at the surface of G 29-38; it allows us to test specific predictions of the convective driving theory, concerning the relationship between the flux and velocity of the modes. In the convective driving mechanism described by Brickhill (1983) and Goldreich & Wu (1999), driving occurs because of the convection zone’s response to the flux perturbations. From this interaction, the flux variations are distorted while the velocities basically traverse the convection zone undiminished. Having both velocity and flux measurements of the pulsation modes, we are able to test the convective driving theory by comparing our data with the analytic predictions of Goldreich & Wu (1999) and the numerical model of Wu & Goldreich (1999).

We have presented the frequency, amplitudes and phases of all seven extracted modes in Table 1. Of these modes, the first four have been previously observed in this star (Kleinman et al. 1998; van Kerkwijk et al. 2000). To see the relationship between the two measurements of the modes, we calculated the relative amplitude,  $R_v = (A_v/\omega)/A_L$ , and the difference between the velocity and flux phases,  $\Delta\Phi = \Phi_v - \Phi_L$ , in accordance with the conventions used by van Kerkwijk et al. (2000). The relative amplitude is a ratio of the velocity amplitude ( $A_v$ ), scaled by the radian frequency ( $\omega = 2\pi f$ ), and the flux amplitude ( $A_L$ ); by including the frequency,  $R_v$  depends only on  $\ell$ , and not on frequency, for adiabatic pulsations (see Dziembowski 1977; Clemens et al. 2000). Only  $\Delta\Phi$  of the first three modes were confidently measured and have values around  $50^\circ$ . The other modes have such low flux amplitudes that the fitted phases could have been easily swayed by noise. Both the relative amplitudes and the phase differences have values similar to the previous measurements of this star (van Kerkwijk et al. 2000). The  $R_v$  range from 10 to 20  $Mm/rad$ ; none is as high as the mode identified as  $\ell = 2$  by van Kerkwijk et al. (2000) and Clemens et al. (2000) ( $R_v = 27 \pm 11 Mm/rad$  for the 777 s mode). Hence, these modes likely have a spherical degree of one, as expected from the conclusions of Kleinman et al. (1998), and measured directly for F1, F2 and F3 by

Clemens et al. (2000).

We can interpret some of these measurements in the context of the analytical theory of the convective driving mechanism (Goldreich & Wu 1999). During an adiabatic pulsation, the maximum velocity occurs a quarter cycle after the flux maximum. However, the large heat capacity of the convection zone alters this basic picture by bottling up heat, thereby reducing the amplitude and delaying the phase of the flux perturbations. This will decrease the difference between the phases of the velocity and flux maxima and increase the ratio between the velocity and flux amplitudes.

Our measurements agree (see Table 1) with these basic predictions of the model; we observe the values of  $\Delta\Phi$  to be less than  $90^\circ$  and  $R_v$  is larger than expected for an adiabatic mode (see van Kerkwijk et al. 2000). We can also specifically compare our data to the model since Wu & Goldreich (1999) calculated their model for a star similar to G 29-38. For an 800 s mode on a 12,160 K star with  $\omega\tau_{th} = 0.8$ , their model shows a phase difference of  $55^\circ$  and relative amplitude of  $16 Mm/rad$ . The 818 s mode measured by van Kerkwijk et al. (2000) confirmed this prediction ( $\Delta\Phi = 44^\circ \pm 19^\circ$ ;  $R_v = 11 \pm 4 Mm/rad$ ). Our measurements of F1 at 817 s mode also agree within the errors to the model calculations. For a graphical comparison, Figure 7 plots our data along with the results of this model.

Another result of the convective driving mechanism (Goldreich & Wu 1999) is the frequency dependence of the interaction between the convection zone and the temperature variations. For larger values of the product of the thermal adjustment time,  $\tau_c$ , and the radian frequency,  $\omega$ , the convection zone has a larger effect on the flux variations. In fact, convective driving can only cause overstability of a mode when the inequality  $\omega\tau_c \geq 1$  is satisfied. As such, we are able to determine a low estimate of the thermal adjustment time from the longest period mode ( $\tau_c \geq 130$  s).

From this  $\omega\tau_c$  dependence, we expect frequency trends in the relative amplitude and phase difference. With increasing frequency, more flux is absorbed, reducing the measured flux amplitude ( $A_L$ ) with respect to the distance the material travels on the star ( $A_v/\omega$ ). Thus, the relative amplitude should increase. Also, with smaller periods, the flux variations experience more phase delay and the difference between the velocity and flux phases become smaller and farther from  $90^\circ$ . Goldreich & Wu (1999) quantifies these trends with expressions for the attenuation and phase delay of the flux variations. The observed flux amplitude is attenuated by the factor  $(1 + (\omega\tau_c)^2)^{-1/2}$  and the flux phase is delayed by  $\arctan(\omega\tau_c)$ . Thus, because of the presence of  $\omega\tau_c$  in these expressions, larger frequencies in the same star should have larger values of  $R_v$  and smaller values of  $\Delta\Phi$ .

Figure 7 shows our measurements of  $R_v$  and  $\Delta\Phi$  as a function of frequency for the purpose of looking for these trends. Neither plot of the data appears to behave as expected, basically showing no obvious variations with frequency. Unfortunately, the comparison to the model is drastically limited by the size of our errors. This is especially notable for modes F4, F5 and F6. Their flux amplitudes are likely inflated by noise and thus, the values for  $R_v$  are underestimated. For this reason, we indicate lower limits for these modes in Figure 7. To compare the measurements with the model we have plotted the trend in  $R_v$  expected by theory in Figure 7. The predicted trend is not apparent in our data. However, because of our large error bars we cannot rule it out. We are not the first to fail to detect the trend; time-resolved spectra of HS 0507+0434B (Kotak et al. 2002) failed to show the predicted trend for  $R_v$  and showed the opposite trend for  $\Delta\Phi$ .

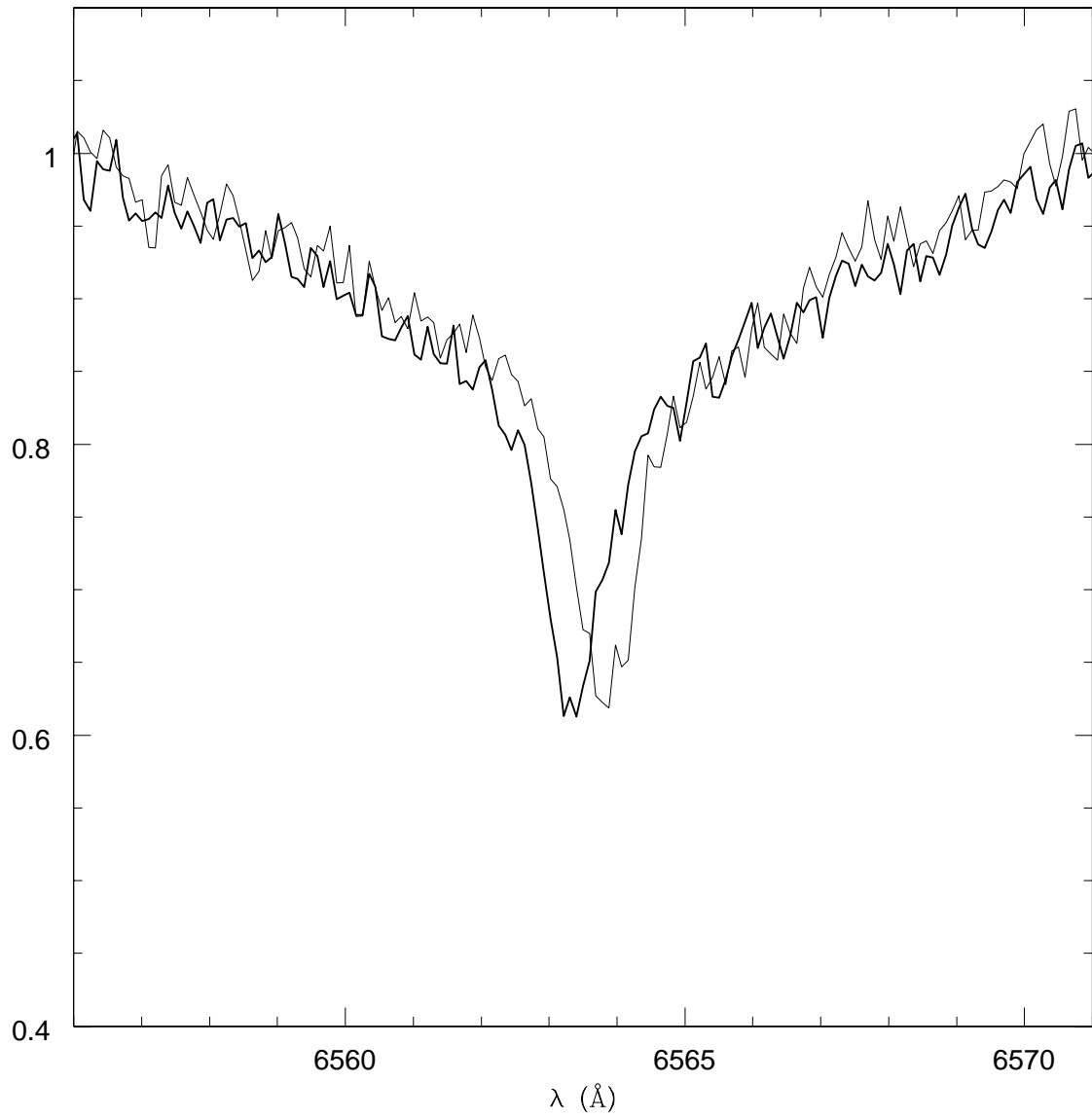


Fig. 6.— The average of 30 blue shift spectra (thick line) and 30 red shift spectra (thin line). The spectra included in each average is measured with a red or blue shift greater than 6.9 km/s.

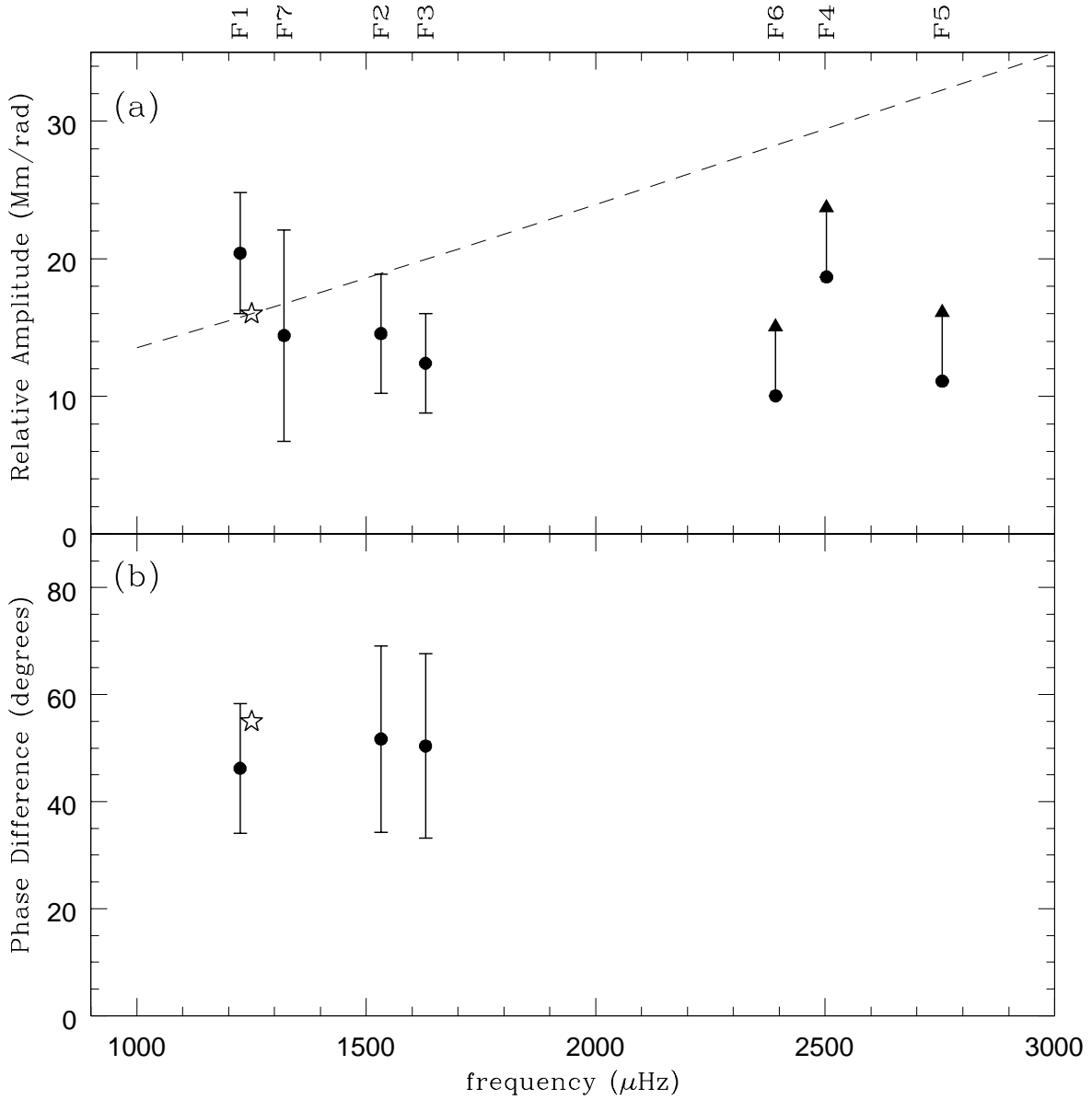


Fig. 7.— A plot of the relative amplitude  $R_v$  (**a**), and the phase difference  $\Delta\Phi$  (**b**) versus frequency for each mode. The star in each plot represents the prediction made by Wu & Goldreich (1999) with their nonadiabatic calculations of g-modes. The dashed line represents the increase in  $R_v$  expected from the predictions of Goldreich & Wu (1999) (for  $\tau_c = 250$  s).

## 5. The Combination Frequency in the Velocity Curve

The analytic theory presented by Goldreich & Wu (1999) makes specific predictions about the existence and behavior of combination frequencies in the Fourier transforms of ZZ Ceti light curves. In their simplest models, which do not incorporate the effects of changing convection zone thickness during pulsation cycles, the flux variations at the photosphere are a diminished and delayed version of the variations that occur at the base of the convection zone. The size of the diminution and delay for a given mode is dependent on the thermal adjustment time of the convection zone and the mode frequency. As long as neither of these change, the effects are linear and do not generate combination frequencies (assuming the variations at the convection base are sinusoidal). However, as first Brickhill (1983) and later Wu (2001) point out, this is unrealistic. The modes in ZZ Ceti are large enough to substantially increase the surface temperature of the star. Equilibrium models of hotter ZZ Ceti stars have thinner surface convection zones, suggesting that pulsating stars will have thinner convection zones at pulsation maxima than at minima. The detailed calculations of Brickhill (1992) and Ising & Koester (2001) confirm this suggestion. The effect of this change in convection zone thickness is that the flux is less diminished at maximum than at minimum, i.e. the maxima rise higher above the mean flux than the minima descend below it. This property of the models corresponds qualitatively, and often quantitatively, to the behavior of the light curves we see.

In the Fourier transforms, this behavior of the models predicts combination frequencies and harmonics that are nearly in phase with the modes that generate them, a condition written by Vuille (2000b) as  $\phi_r = \phi_{1,2} - (\phi_1 + \phi_2) \approx 0$ , where  $\phi_{1,2}$  is the phase of the combination and  $\phi_1$  and  $\phi_2$  are the phases of its parent modes. The analysis of modes in G 29-38 by Vuille (2000b) shows that the combination frequencies show  $\phi_r$  near an average value of  $22^\circ$ , consistent with their harmonic distortions being generated by the changing convection zone depth, just as the models describe.

The prediction of the models with respect to velocity combinations is harder to discern. Brickhill (1990) and Wu (2001) assume that turbulent viscosity in the convection zone enforces uniform velocity with depth. Thus their model convection zone does not introduce any delay or diminishment of velocities between its base and the surface, so the mechanism responsible for the distorted light curves does not operate on the velocities. Furthermore, Brickhill (1992) argues that second order perturbations to the horizontal motions should be smaller than the linear perturbations by a factor of 10 or more. Based on this argument, Brickhill *imposes* sinusoidal pressure variations and displacements in his model. Because his model does not allow feedback that could alter the imposed variations, it can never exhibit non-sinusoidal horizontal motions. The models of Ising & Koester (2001) and the analytic treatment of Wu (2001) also assume sinusoidal pressure variations and have no feedback. Consequently, none of the published models have any ability to predict the shape of velocity curves: they only reap what they have sown.

Fortunately, the phase of our velocity combination offers a clue to its origin. If we define the relative phase in the same way as for the flux combinations, then we find from Table 1 that  $\phi_{r,velocity} = \phi_{F5} - (\phi_{F1} + \phi_{F2}) = -95^\circ$ . A phase difference of  $-95^\circ$  suggests a simple possibility. If the horizontal *displacements* are distorted in the same way as the flux curves we observe, then they would generate combination frequencies with  $\phi_{r,displacement} \approx 0$ . The velocities we measure are the time derivatives of the displacements, and the derivative introduces a  $90^\circ$  phase shift in both of the parent frequencies and in the combination, so we expect  $\phi_{r,velocity} \approx 270^\circ = -90^\circ$ . That is, the relative phase of the velocity combination frequency we have measured is close to the value we expect if the horizontal displacements vary in a manner similar to the flux variations.

This does not answer the question of why the measured displacements should show this behavior. The



observations require that in the half cycle where horizontal displacements are directed toward a surface anti-node, material travels farther from its equilibrium position than it does in the half cycle where displacements are directed toward a node. Perhaps this is an overlooked consequence of the strongly non-sinusoidal temperature variations at the pulsation anti-nodes. Alternatively, it is possible that the uniform (with depth) horizontal velocities enforced by the convection zone introduce a non-sinusoidal component into the velocities as the thickness of the convection zone changes during a pulsation cycle. In the models, the convection zone "averages" the horizontal velocities to a value somewhere between the values that would be present at its base and surface if turbulent viscosity did not enforce uniform horizontal motion (see Figure 5 of Wu & Goldreich (1999)). As the convection zone changes depth, and perhaps even entirely evaporates at the anti-nodes, the effect on the surface motions might change during a cycle, yielding a non-sinusoidal component. However, it is not clear that the relative phase of this component would match the relative phase of the combination peak we have measured.

We can speculate further, but we are far from understanding the origin of the velocity combination F5. First, we cannot make any statistical arguments on the basis of one mode, so we cannot rule out the possibility that F1, F2, and F5 represent an example of resonant mode coupling as described by Wu & Goldreich (2001) and Dziembowski (1982), in which case the phase relationship measured is accidental. Second, without actual calculations extending the works of Brickhill (1983, 1992), Wu (2001) and Ising & Koester (2001), we do not know what detailed models will predict for the phase of velocity combination modes. Nonetheless, we think the speculation we have presented represents the most fruitful immediate direction for observational and theoretical investigations.

## 6. The Spectral Profile of G 29-38

The time-resolved, high resolution spectroscopy of G 29-38 enables us to explore a mystery concerning the observed line profile of the  $H\alpha$  core of ZZ Ceti. Our data are similar to the observations made by Koester et al. (1998) to measure the rotation rate of DA white dwarf stars except that we have a time-series of exposures of 50 s each instead of one, hour long exposure. Thus, the average of our spectra can confirm their rotationally broadened fit to G 29-38, while the short exposure times allow us to test the possibility that the line shape is altered by the pulsational shifts.

Koester et al. (1998) modeled the  $H\alpha$  line to determine the rotation rates of 28 DA white dwarfs. They found that the majority of the stars have small rotation rates with an upper limit of 15 km/s. However, the  $v \sin i$  for each of the three ZZ Ceti stars, including G 29-38, is between 30 and 45 km/s. This fitted velocity drastically exceeds what is expected from rotational splitting (Kleinman et al. 1998), and it seems unlikely that white dwarf stars spin-up as they cool into the instability strip. On close inspection of the data obtained by Koester et al. (1998), the shape of  $H\alpha$  core resembles the zero rotation model except for the depth of the line; the model is almost 20% deeper than the spectrum. A large rotation model successfully fits the depth of the line, but appears to be too broad.

Reassuringly, our average spectrum is identical in shape and depth to the 1-hour exposure of Koester et al. (1998). We fit the same rotationally broadened model used in Koester et al. (1998) to our average spectrum and present the results in Figure 9. Again, the best fit, with  $v \sin i$  of  $42.2 \pm 3$  km/s, is able to emulate the depth of the line, but does not fit the width as well as the zero rotation model. With the increased signal-to-noise of our average spectrum, we can confidently confirm the statement made by Koester et al. (1998) that the large rotation fit is forced by the shallow cores and is too wide for the observations. To

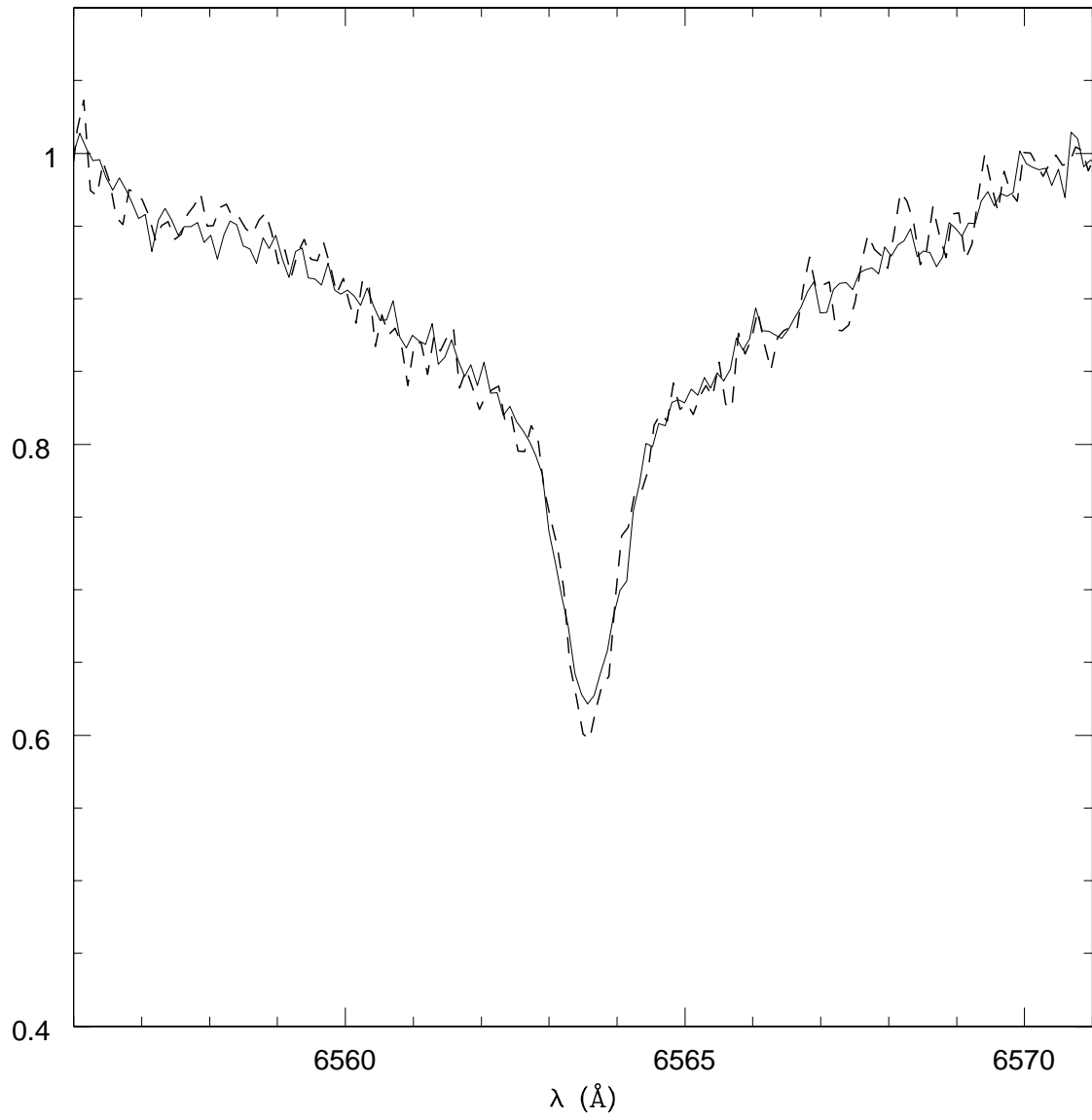


Fig. 8.— The average of the spectra with small measured velocities (dashed line) overplotted on the average spectrum (solid line).

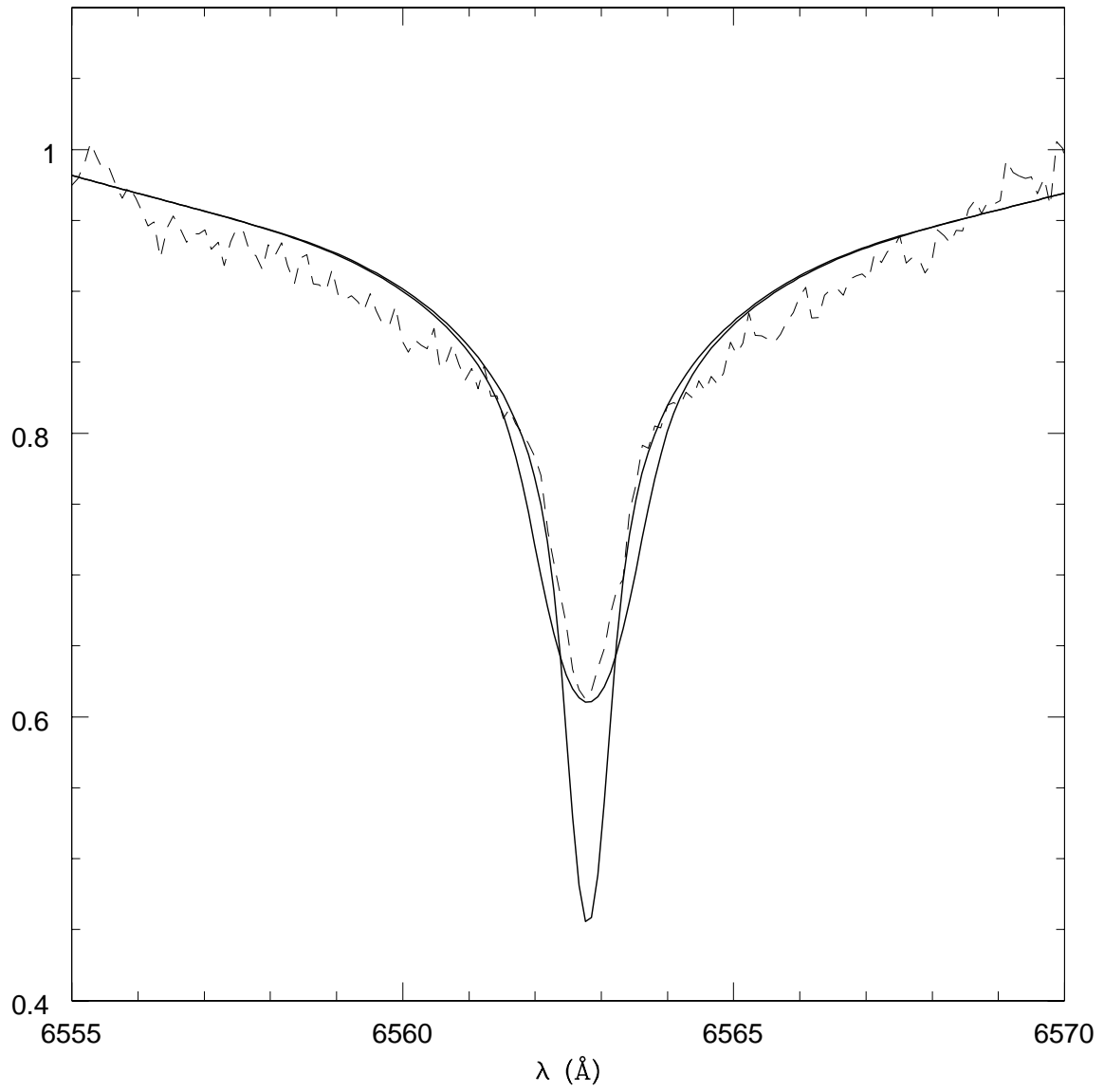


Fig. 9.— Fits to the average spectrum. The deep core is the model with zero rotational velocity and the shallow core is the rotational broadened model corresponding to a velocity of  $42.2 \pm 3$  km/s.

quantify the discrepancy between the model and the observations we calculate a reduced chi-square of 3 for the fit using an error of 1.6% (estimated from the observational scatter outside the line core) for the average spectrum in Figure 8. The odds that our rotationally broadened model would be so poor a fit to the data by chance alone are very small. Accordingly, we can discard the rotational model; it is too wide to properly fit the data.

Because rotation fails to account for the line shape, we tested the hypothesis that the altered shape of the spectral line is due to pulsation. As shown above, the g-mode pulsations create small Doppler shifts of the line. Since the exposure time used by Koester et al. (1998) is much longer than the period of the modes, the spectrum could be smeared-out by these velocity shifts. If true, each of our spectra will have a line shape with a deeper core.

Because the signal-to-noise of each individual spectrum is not sufficient to examine a change in the line shape, we reduced the noise by averaging spectra with similar measured velocities. The high and low velocity averages, presented earlier to show the spectral shifts (Figure 6), have approximately the same shape as the average spectrum. We also averaged together 30 spectra with velocities between 1.1 and -1.1 km/s to see the line shape unaffected by the spectral shifts. Figure 8, a plot of the small velocity and total averages, demonstrates how little change occurs in the line shape when the spectra with large velocities are excluded.

The small velocity average shows a slightly deeper core; however, this 2% drop is not nearly large enough to reproduce the zero velocity spectral line in Figure 9. By convolving the low velocity average spectrum with a gaussian whose fwhm is equal to the root-mean-square of the velocity curve (6.8 km/s or 0.15 Å), we see that this 2% drop is exactly what is expected for the size of the pulsation velocities. In fact, we would need to convolve the zero-rotation spectrum with a velocity four times larger than measured to achieve the average spectrum line depth; this convolved spectrum is also too wide to emulate the observed spectral line. Though the pulsation motions do present themselves as Doppler shifts, these shifts do not have a significant effect on the shape of the time-averaged H $\alpha$  spectrum.

Our high signal-to-noise spectra have now eliminated two possible explanations for the line shape of the H $\alpha$  core of ZZ Ceti: rotation and pulsation. Our average spectrum convincingly demonstrates that the rotationally broadened line does not fit the line profile. An average spectrum created by binning spectra with similar velocities did not result in a significantly different line profile, eradicating the possibility that the pulsations truncate an intrinsically deeper line. The only remaining explanation is that some aspect of the stellar atmosphere must not be accounted for in the model spectrum. The shallow core suggests that the outer atmosphere is hotter than expected. We do not know a good physical reason for this, and therefore, must leave the question concerning the ZZ Ceti line shapes unanswered.

## 7. Conclusions

We have introduced high resolution, time-resolved spectroscopy to the study of cool white dwarf pulsators with observations of the DAV G 29-38. This technique enabled us to measure the line-of-sight velocities and the flux variations associated with the g-mode pulsations. Despite the low signal-to-noise for each individual spectrum, the fits to the H $\alpha$  core successfully reveal the Doppler shift of each spectrum, revealing seven velocity modes with corresponding flux modes. The obvious spectral shifts and the frequency correlation between velocity and flux modes confirm the previous velocity detections in G 29-38 by van Kerkwijk et al. (2000) with low-resolution spectra.

As with the low resolution data, we compared the amplitudes and phases of the velocity and flux measurements of each mode. To that end, we calculated the relative amplitude  $R_v$  and phase difference  $\Delta\Phi$  of each mode. Overall, these values agree with the previous measurements of G 29-38 (van Kerkwijk et al. 2000). The value of  $\Delta\Phi$  for the three largest modes shows that the velocity maximum leads the flux maximum by less than a quarter cycle, as expected. The values of  $R_v$  are in the same range as the previous measurements. None of the values are as high as the mode identified to be  $\ell = 2$  (Clemens et al. 2000), indicating that all the modes measured here have a spherical degree of one.

We also compared the relative amplitude and phase difference with the predictions made by the models of Goldreich & Wu (1999) and Wu & Goldreich (1999) which describe the pulsations on ZZ Ceti stars in the context of a convective driving theory. The values of  $R_v$  and  $\Delta\Phi$  agree with the model; however, they do not show the trend with frequency predicted from the convection zone’s interaction with the flux variations. Considering the size of our errors, this lack of agreement has questionable value. Other observations (Kotak et al. 2002; van Kerkwijk et al. 2000) have also failed to see the predicted trends, indicating a possible problem with the convective driving model.

Perhaps not surprisingly, our new technique has uncovered a new phenomenon— a velocity combination frequency. Although it is dangerous to generalize from a single detection, it appears that the surface velocity variations for large amplitude ZZ Ceti stars can experience harmonic distortion just as the flux variations do. We have discussed this as the product of an underlying distortion in the horizontal displacements that has properties similar to the distortions in the flux variations. Unfortunately, none of the existing models are capable of predicting, or even reproducing, this behavior. We believe that some effort in this direction could resolve many mysteries surrounding G 29-38 and the entire class of ZZ Ceti pulsators.

Finally, we investigated the effects of pulsation velocities on the shape of the  $H\alpha$  line core. The Doppler shifts could potentially broaden the line when observed with a long exposure. Our short exposure times enabled us to examine the line shape of the NLTE core of  $H\alpha$  without this effect. We discovered that removing the spectra with large Doppler shifts from the average line did not significantly alter the shape of the line, indicating that the pulsations are not causing the broadened profile. Rotation, another notorious line broadener, also appears unlikely because the best rotation model failed to fit the width of the line while yielding an unbelievably large velocity (Koester et al. 1998). With both pulsation and rotation eliminated as potential answers, the cause for the truncated shape of the  $H\alpha$  core remains a mystery.

The observations for this paper were taken at the W. M. Keck Observatory, which is operated by the California Association for Research in Astronomy, a scientific partnership among the California Institute of Technology, the University of California, and the National Aeronautics and Space Administration. It was made possible by the generous financial support of the W. M. Keck Foundation. We also recognize support from the National Science Foundation through grant AST-0094289 and from the DLR (Deutsches Zentrum für Luft- und Raumfahrt) through grant 50 OR96173. C. Clemens acknowledges the Alfred P. Sloan Foundation, S. Thompson would like to thank the North Carolina Space Grant Consortium for their support and M. H. van Kerkwijk acknowledges support by a fellowship of the Royal Netherlands Academy of Science.

## REFERENCES

- Bradley, P. A., & Kleinman, S. J. 1997, in European White Dwarf Workshop, White Dwarfs, ed. J. Isern, M. Hernanz, & E. Garcia-Berro (Dordrecht: Kluwer), 445
- Brassard, P., Fontaine, G., & Wesemael, F. 1995, *ApJS*, 96, 545
- Brickhill, A. J. 1983, *MNRAS*, 204, 537
- Brickhill, A. J. 1990, *MNRAS*, 246, 510
- Brickhill, A. J. 1991, *MNRAS*, 251, 673
- Brickhill, A. J. 1992, *MNRAS*, 259, 519
- Clemens, J. C., van Kerkwijk, M. H., & Wu, Y. 2000, *MNRAS*, 314, 220
- Dolez, N., & Vauclair, G. 1981, *A&A*, 102, 375
- Dziembowski, W. 1977, *Acta Astron.*, 27, 203
- Dziembowski, W. 1982 *Acta Astron.*, 32, 147
- Dziembowski, W. & Koester, D. 1981, *A&A*, 97, 16
- Goldreich, P. & Wu, Y. 1999, *ApJ*, 511, 904
- Horne, K. 1986, *PASP*, 98, 609
- Horne, J. H. & Baliunas, S. L. 1986, *ApJ*, 302, 757
- Ising, J. & Koester, D. 2001, *A&A*, 374, 116
- Kepler, S. O. 1993, *Baltic Astron.*, 2, 515
- Kleinman, S. J. et al. 1998, *ApJ*, 495, 424
- Koester, D., Dreizler, S., Weidemann, V., and Allard, N. F. 1998, *A&A*, 338, 612
- Kotak, R., van Kerkwijk, M. H., & Clemens, J. C. 2002, *A&A*, 388, 219
- O'Donoghue, D., Warner, B., & Cropper, M. 1992, *MNRAS*, 258, 415
- Oke, J. B., et al. 1995, *PASP*, 107, 375
- Tody, D. 1986, *Proc. SPIE*, 627, 733
- van Kerkwijk, M. H., Clemens, J. C., & Wu, Y. 2000, *MNRAS*, 314, 209
- Vogt, S. S., et al. 1994, *SPIE*, 2198, 362
- Vuille, F. 2000a, *MNRAS*, 313, 170
- Vuille, F. 2000b, *MNRAS*, 313, 179
- Vuille, F. & Brassard, P. 2000, *MNRAS*, 313, 185

Warner, B. & Nather, R. E. 1970, *MNRAS*, 147, 21

Winget, D. E., et al. 1990, *ApJ*, 357, 630

Winget, D. E., Van Horn, H. M., Tassoul, M., Hansen, C. J., Fontaine, G., & Carroll, B. W. 1982, *ApJ*, 252, L65

Wu, Y. 2001, *MNRAS*, 323, 248

Wu, Y. & Goldreich, P. 1999, *ApJ*, 519, 783

Wu, Y. & Goldreich, P. 2001, *ApJ*, 546, 469

Table 1. The amplitudes, phases,  $R_v$ , and  $\Delta\Phi$  for each mode.

mode	P(s)	$f(\mu\text{Hz})$	$A_v(\text{km/s})$	$\Phi_v$ ( $^\circ$ )	$A_L$ (%)	$\Phi_L$ ( $^\circ$ )	$R_v$ (Mm/rad) <sup>†</sup>	$\Delta\Phi$ ( $^\circ$ )
F1	816	$1224.9 \pm 3.0$	$4.53 \pm 0.44$	$270 \pm 6$	$2.88 \pm 0.55$	$224 \pm 11$	$20.4 \pm 4.4$	$46 \pm 12$
F2	653	$1532.1 \pm 4.6$	$2.95 \pm 0.44$	$216 \pm 9$	$2.11 \pm 0.54$	$165 \pm 15$	$14.5 \pm 4.3$	$52 \pm 17$
F3	614	$1629.1 \pm 4.8$	$2.79 \pm 0.44$	$304 \pm 9$	$2.20 \pm 0.54$	$253 \pm 14$	$12.4 \pm 3.6$	$50 \pm 17$
F4	399	$2503.4 \pm 4.7$	$2.84 \pm 0.44$	$177 \pm 9$	$0.97 \pm 0.54$	$12 \pm 32$	$18.7 \pm 10.8$	$165 \pm 33$
F5*	363	$2754.9 \pm 6.7$	$1.97 \pm 0.43$	$31 \pm 13$	$1.02 \pm 0.54$	$35 \pm 30$	$11.1 \pm 6.4$	$-5 \pm 33$
F6	418	$2391.9 \pm 8.5$	$1.57 \pm 0.44$	$280 \pm 16$	$1.04 \pm 0.54$	$4 \pm 30$	$10.0 \pm 5.9$	$275 \pm 34$
F7	757	$1321.1 \pm 9.3$	$1.48 \pm 0.45$	$137 \pm 17$	$1.23 \pm 0.54$	$260 \pm 25$	$14.4 \pm 7.7$	$-124 \pm 31$

\*F5 is the combination mode, its frequency is the sum of F1 and F2.

<sup>†</sup>The reader may prefer the more intuitive units of  $10\text{km}/\text{rad}/\%$ .

Note. — For each mode,  $R_v = (A_v/\omega)/A_L$  and  $\Delta\Phi = \Phi_v - \Phi_L$ . The reported errors reflect a reduced chi-squared of 1 for the least-squares fits to the flux and velocity curves.